Quantitative Optical Coherence Tomography Findings in Various Subtypes of Neovascular Age-Related Macular Degeneration

Sandra Liakopoulos,[1,2] *Sharel Ongchin,*[1] *Alok Bansal,*[1] *Sandeep Msutta,*[1] *Alexander C. Walsh,*[1] *Paul G. Updike,*[1] *and Srinivas R. Sadda*[1]

Purpose. To compare the volume of various spaces visible on optical coherence tomography (OCT) images in different angiographic lesion subtypes of neovascular age-related macular degeneration (AMD).

Methods. Sixty-six cases of previously untreated, active subfoveal choroidal neovascularization (CNV) associated with AMD were retrospectively collected. CNV lesions were classified as occult with no classic CNV, minimally classic CNV, predominantly classic CNV, or CNV lesions with associated retinal angiomatous proliferation (RAP). Corresponding OCT image sets were analyzed by trained graders using previously validated custom software that allows manual placement of boundaries on OCT B-scans. Spaces delineated by these boundaries included the neurosensory retina, subretinal fluid, subretinal tissue, and pigment epithelial detachments (PEDs). Volume measurements were calculated by the software and compared among groups.

Results. Minimally and predominantly classic CNV membranes demonstrated subretinal tissue on OCT in all cases and appeared to show a significantly greater volume of subretinal tissue than did the occult membranes. Subretinal fluid was present in all the predominantly classic cases. A PED was visible in all the occult CNV cases in our study, demonstrating less retinal thickening and significantly greater PED volumes than minimally and predominantly classic CNV lesions. Lesions associated with RAP showed the highest percentage of cystoid spaces.

Conclusions. OCT and angiography provide complementary information regarding CNV lesions. Quantitative analysis of OCT images allows for an improved understanding of the anatomic characteristics of angiographically defined CNV lesion subtypes. (*Invest Ophthalmol Vis Sci.* 2008;49:5048–5054) DOI:10.1167/iovs.08-1877

Age-related macular degeneration (AMD) is the most common cause of blindness in North America and Europe.[1] In neovascular AMD, two different patterns of choroidal neovascularization (CNV) have been defined according to their appearance on fluorescein angiography (FA): classic CNV and occult CNV.[2] Occult CNV has been further subdivided into fibrovascular pigment epithelial detachment (FVPED) and late leakage of undetermined source (LLUS). Recently, the presence of retinal angiomatous proliferation (RAP) or retinal anastomosis to the lesion (RAL) has been identified in some cases of CNV.[3]

Classic CNV, occult CNV, and RAP are believed to have different characteristics with respect to the progression of the disease over time and the impact on visual function. Large randomized clinical trials have demonstrated significant differences in treatment effects in minimally classic CNV (<50% of the lesion occupied by classic CNV), predominantly classic CNV (> 50% of the lesion occupied by classic CNV), and occult with no classic CNV.[2,4,5] The presence of RAP also seems to have an impact on the course of the disease and on the treatment outcome.[3]

Although FA remains an important tool in the diagnosis of CNV lesions, optical coherence tomography (OCT) has become an increasingly important component in the management of patients with neovascular AMD. Retinal thickening, subretinal fluid, subretinal tissue, and pigment epithelial detachments (PEDs) are all well visualized on OCT B-scans and have permitted the study of the anatomic features of CNV lesions. Classic CNV is believed to correspond frequently to histologic type 2 CNV (CNV between retinal pigment epithelium [RPE] and retina),[6,7] which may appear on OCT as subretinal tissue.[8–12] Occult CNV is believed to correspond to histologic type 1 CNV (between Bruch's membrane and RPE),[6,7] which may in FVPED (but not in LLUS) appear as a PED on OCT.[8–12] Leakage on FA caused by active CNV usually appears as intraretinal, subretinal, or sub-RPE fluid accumulation on OCT.[9–12]

To date, the appearance of the different lesion types on OCT are only qualitatively described.[9–12] In this study, we analyzed OCT images of eyes with neovascular AMD using computer-assisted manual grading software to quantify various spaces visible on OCT images for a more precise comparison of the characteristics of different angiographic CNV lesion subtypes.

Methods

Data Collection

Data from 66 eyes of 66 consecutive patients who were about to enter therapy for neovascular AMD were retrospectively collected. To be eligible for the study, eyes were required to have previously untreated, active subfoveal CNV due to AMD and StratusOCT (Carl Zeiss Meditec, Inc., Dublin, CA) imaging, as well as FA imaging performed on the same date. In addition, the entire CNV lesion as defined on FA had to fall within a 6-mm-diameter circle centered on the fovea. Active CNV was defined as the presence of hemorrhage or evidence of vision loss (of at least one line of Snellen acuity) or lesion growth within the prior 3 months.

From the [1]Doheny Image Reading Center, Doheny Eye Institute, Keck School of Medicine of the University of Southern California, Los Angeles, California; and the [2]Department for Vitreoretinal Surgery, Center for Ophthalmology, University of Cologne, Cologne, Germany.

Supported in part by National Eye Institute Grants EY03040 and R01 EY014375 and RetinoVit Stiftung Cologne, Germany.

Submitted for publication February 14, 2008; revised May 27, 2008; accepted August 29, 2008.

Disclosure: **S. Liakopoulos**, None; **S. Ongchin**, None; **A. Bansal**, None; **S. Msutta**, None; **A.C. Walsh**, Topcon Medical Systems (P); **P.G. Updike**, None; **S.R. Sadda**, Topcon Medical Systems (P)

The publication costs of this article were defrayed in part by page charge payment. This article must therefore be marked "*advertisement*" in accordance with 18 U.S.C. §1734 solely to indicate this fact.

Corresponding author: Srinivas R. Sadda, Doheny Eye Institute, DEI 3623, 1450 San Pablo Street, Los Angeles, CA 90033; sadda@usc.edu.

Investigative Ophthalmology & Visual Science, November 2008, Vol. 49, No. 11

Approval for the collection and analysis of the data was obtained from the Institutional Review Board of the University of Southern California. The research adhered to the tenets set forth in the Declaration of Helsinki.

Color fundus photographs and FA images were obtained with a camera with an 11-megapixel sensor (Topcon 50IX; Topcon Medical Systems, Paramus, NJ). The standard imaging protocol of the Doheny Imaging Unit was adhered to in all cases, consisting of color stereo pairs of the ETDRS fields 1 and 2, followed by multiple angiographic frames of field 2 during the transit phase, and stereo pairs of field 2 in the mid (<3 minutes) and late (5–10 minutes) phases of the angiogram.

OCT images were obtained using the Radial Lines protocol in which six high-resolution 6-mm B-scans (transverse resolution of 512 A-scans per B-scan) were obtained with a single StratusOCT machine (Carl Zeiss Meditec, Inc.). Although there have been many published reports on OCT in which the Fast Macular Scan protocol was used (with a lower transverse resolution of 128 A-scans per B-scan), the high-resolution Radial Lines protocol has been the standard method used in the Doheny Ophthalmic Imaging Unit due to the enhanced morphologic detail provided. The Fast Macular Scan protocol was used only when photographers were unable to obtain adequate high-resolution images, most commonly in patients with unstable fixation or poor cooperation. Photographers attempted to center the OCT B-scans on the fovea in all cases.

Data for each case were exported to disc by using the export feature available in the system's analysis software (StratusOCT, version 4.0; Carl Zeiss Meditec, Inc.).

Computer-Assisted OCT Grading Software

The software used for OCT analysis (termed OCTOR) was written by Doheny Image Reading Center (DIRC) software engineers to facilitate viewing and manual grading.[13] The OCTOR software is freely accessible at https://www.diesel.la and has been described and validated in previous reports.[13,14] The software imports data exported from the StratusOCT machine and allows the grader to use a computer mouse to draw various boundaries in the retinal cross-sectional images.

After the grader draws the required layers in each of the six OCT B-scans, the software calculates the distance in pixels between the manually drawn boundary lines for each of the various defined spaces. Using the dimensions of the B-scan image, the calculated pixels are converted into micrometers to yield a thickness measurement at each location. The thickness at all unsampled locations between the radial lines is then interpolated to generate a thickness or volume map analogous to the StratusOCT output. The interpolation algorithm and intergrader reproducibility have previously been validated.[13,14]

Analogous to the StratusOCT software, the OCTOR software provides a report showing the calculated thickness and volume values for the nine Early Treatment of Diabetic Retinopathy Study (ETDRS) macular subfields, and the mean and SD of the foveal center point (FCP) thickness (Fig. 1). In contrast to the Stratus output, the OCTOR software provides separate maps for the various macular spaces (e.g., retina, subretinal fluid, subretinal tissue, and PEDs).

Grading Procedure

FA images and OCT scans were analyzed by certified graders (SL, SRS) at the DIRC.[2,14] FAs were viewed and graded using DIRC FA grading

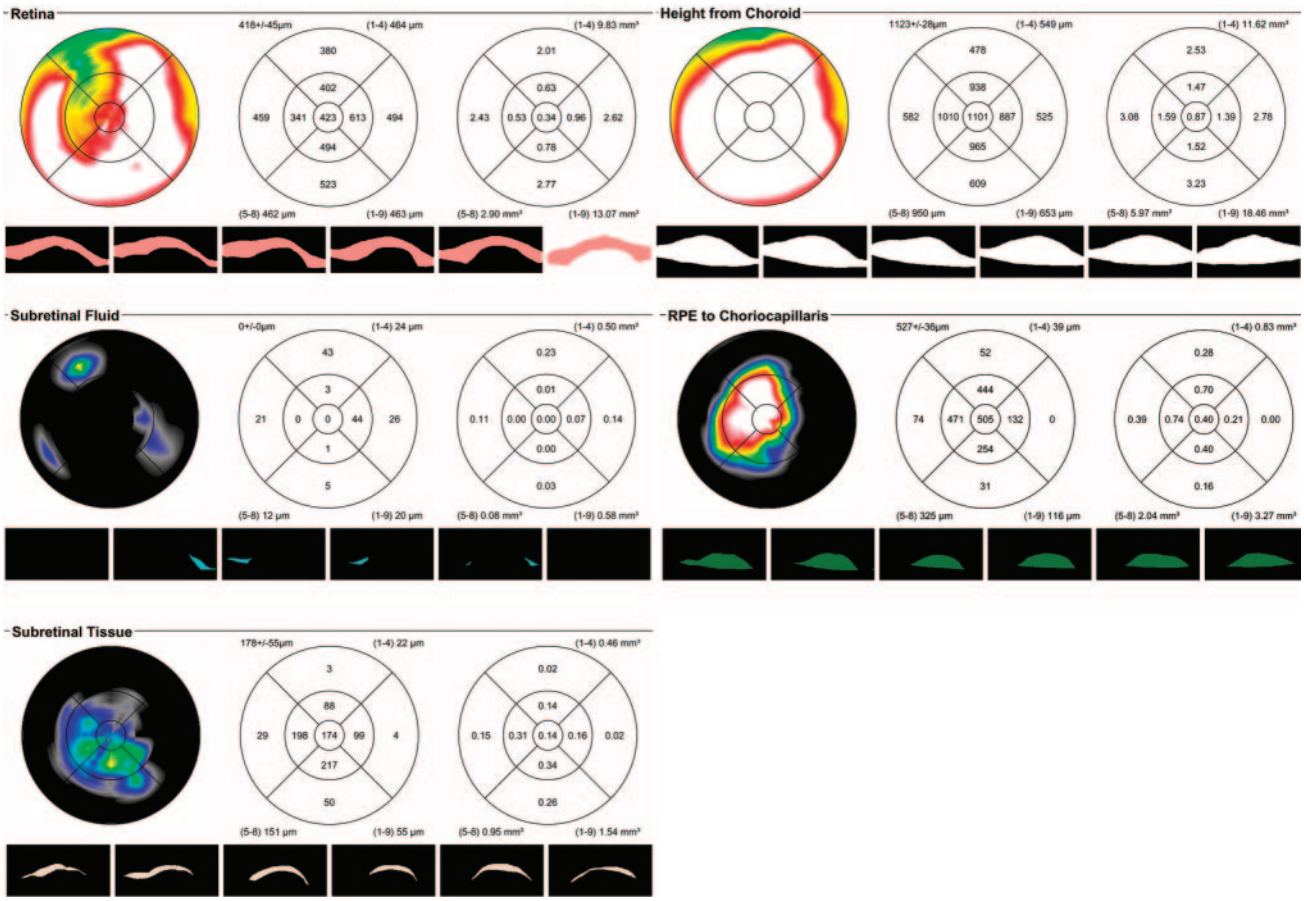

FIGURE 1. OCTOR map demonstrating the volume and thickness of all spaces calculated by the OCTOR software after manual grading of all six OCT B-scans.

TABLE 1. OCT Features in Different Angiographic Lesion Subtypes

Subtype	Occult with No Classic (n = 24)	Minimally Classic (n = 23)	Predominantly Classic (n = 11)	RAP Stage III (n = 8)
Subretinal fluid	19 (79)	21 (91)	11 (100)	4 (50)
Subretinal tissue	7 (29)	23 (100)	11 (100)	7 (88)
Pigment epithelial detachment	24 (100)	16 (70)	5 (45)	7 (88)
Cystoid edema	14 (58)	17 (74)	9 (82)	8 (100)

Data are the number (%) in each lesion subtype group demonstrating the various features.

software equipped with standard planimetric tools to allow calculation of the area and greatest linear dimension (GLD) of any closed-loop figure/structure drawn on computer by the grader with the aid of the computer mouse. CNV lesions were graded according to the modified Macular Photocoagulation Study (MPS) grading protocol used in the TAP and VIP studies.[2] Eyes were classified into four groups according to their appearance on FA: (1) predominantly classic CNV, (2) minimally classic CNV, (3) occult with no classic CNV, and (4) CNV associated with RAP.[2] The area (measured in MPS disc areas) and GLD (measured in mm) of the CNV lesions were calculated. In addition, the presence of hemorrhage and hard exudates on color fundus photography was noted.

OCT B-scans were analyzed using the computer-assisted manual grading software OCTOR.[14] Graders were masked as to the angiographic lesion subtype when analyzing the OCT image set. Boundaries drawn in each of the six OCT B-scans included the internal limiting membrane (ILM), the outer border of the photoreceptors, borders of subretinal fluid and subretinal tissue (if present), the inner surface of the RPE, and the estimated normal position of the RPE layer (in cases with RPE elevation). All boundaries were drawn in accordance with the standard OCT grading protocol of the DIRC.[14] The presence of intraretinal cystoid spaces was also noted.

After grading was completed, the OCTOR software was used to calculate the volume for the various spaces: retina, subretinal fluid, subretinal tissue, and PED. In addition, a combined parameter, the inner retinal surface height from the choroid (IHC), was also calculated as the combination of all four individual spaces.

Statistical Methods

Volumes (in cubic millimeters) for subfields 1 to 9 were collected for each space and each case, and mean and SD values were calculated across all cases. The area of the CNV lesion was measured using TAP grading criteria in each case. The volume values for each case (and for every space) were computed as a ratio by dividing the volume by the area measurement, effectively normalizing the values with respect to lesion area. Values were compared between groups. Statistical analysis was performed using commercially available software (SigmaPlot 2004 for Windows, ver. 9.01; Systat Software Inc., Erkrath, Germany). For the comparison between groups, the ANOVA on ranks test (for comparison between more than two groups), the *t*-test, or the Mann-Whitney rank sum test (for comparison between two groups) was used, depending on whether the data matched the pattern expected in a population with a normal distribution. $P < 0.05$ was considered statistically significant.

RESULTS

Predominantly classic CNV was diagnosed on fluorescein angiography in 11 cases, minimally classic CNV in 23 cases, occult with no classic CNV in 24 cases, and CNV associated with RAP in 8 cases.

OCT measurements for all subtypes are summarized in Tables 1 and 2. The different CNV lesion subtypes showed the following characteristics on OCT.

Predominantly classic CNV was associated with retinal thickening (defined as total retinal volume greater than 7 mm^3) and subretinal fluid accumulation on OCT in all 11 cases (100%; mean retinal volume 8.47 ± 1.78 mm^3, mean volume of subretinal fluid 0.24 ± 0.20 mm^3). Cystoid spaces were present in nine cases (82%). Subretinal tissue was detected on OCT in all cases (100%; mean subretinal tissue volume 0.56 ± 0.55 m^3). Five eyes also demonstrated additionally PEDs (45%, mean PED volume 0.38 ± 0.97 mm^3). In three of the five cases with PED on OCT (60%), occult CNV could be identified on FA as a lesion component, whereas none of the eyes without PED on OCT showed occult components on FA.

Minimally classic CNV (Fig. 2) was associated with retinal thickening in 20 of 23 cases (87%, mean retinal volume 7.86 ± 0.91 mm^3), retinal cystoid spaces in 17 eyes (74%) and subretinal fluid accumulation in 21 cases (91%, mean volume 0.5 ±

TABLE 2. Volume Measurements of Various Spaces on OCT B-Scans

OCT Parameter	Occult with No Classic (n = 24)	Minimally Classic (n = 23)	Predominantly Classic (n = 11)	RAP Stage III (n = 8)
Retina				
Mean ± SD	7.62 ± 0.72	7.86 ± 0.91	8.47 ± 1.78	8.54 ± 1.76
(min-max)	(6.28–9.33)	(6.49–9.98)	(7.01–13.07)	(6.80–12.39)
Subretinal fluid				
Mean ± SD	0.24 ± 0.50	0.50 ± 0.59	0.24 ± 0.20	0.42 ± 0.69
(min-max)	(0.00–2.39)	(0.00–2.41)	(0.01–0.58)	(0.00–1.87)
Subretinal tissue				
Mean ± SD	0.07 ± 0.14	0.37 ± 0.41	0.56 ± 0.55	0.11 ± 0.10
(min-max)	(0.00–0.51)	(0.01–1.76)	(0.07–1.56)	(0.00–0.23)
PED				
Mean ± SD	0.86 ± 0.73	0.32 ± 0.36	0.38 ± 0.97	0.59 ± 0.62
(min-max)	(0.01–2.78)	(0.00–1.21)	(0.00–3.27)	(0.00–1.75)
Inner retinal height from choroid				
Mean ± SD	8.79 ± 1.28	9.05 ± 1.60	9.64 ± 3.14	9.66 ± 2.01
(min-max)	(6.72–12.27)	(6.87–13.33)	(7.51–18.46)	(7.70–13.57)

Data are in cubic millimeters.

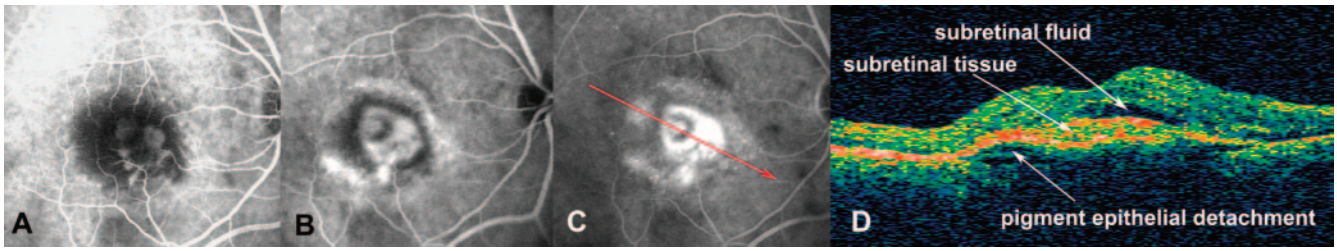

FIGURE 2. Early phase (**A**), mid phase (**B**), and late phase (**C**) FA of a case of minimally classic CNV. (**D**) The corresponding OCT B-scan (scan direction marked by *red arrow* in (**C**)) demonstrated subretinal fluid, subretinal tissue, and a PED. OCT illustrated that the PED (presumably corresponding to type 1 CNV) continued beneath the subretinal tissue (presumably corresponding to type 2 CNV), whereas on FA, only a circular area of stippled hyperfluorescence was visible, indicating occult CNV, and the central part of the PED was hidden beneath classic CNV.

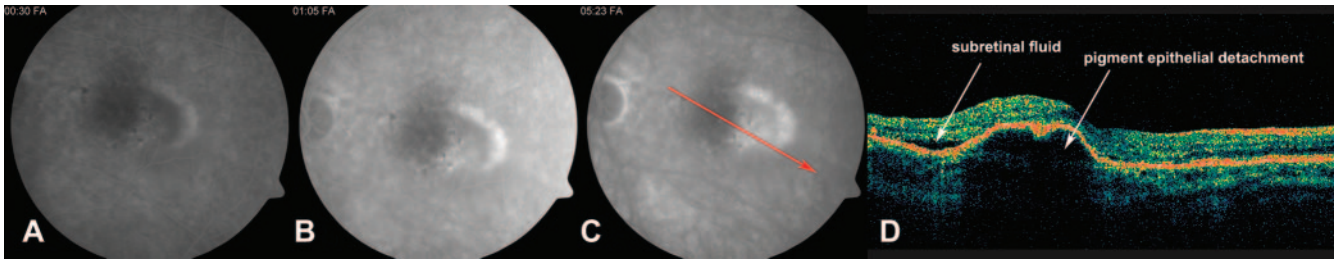

FIGURE 3. Early phase (**A**), mid phase (**B**), and late phase (**C**) FA of a case of occult with no classic CNV. (**D**) The corresponding OCT B-scan (scan direction marked by *red arrow* in (**C**)) shows a PED and subretinal fluid.

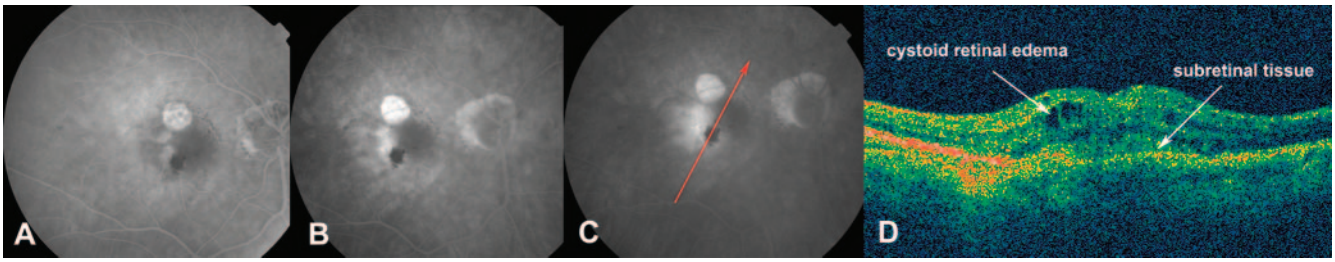

FIGURE 4. Early phase (**A**), mid phase (**B**), and late phase (**C**) FA of a case demonstrating a stereoscopically visible RAP connected to occult choroidal neovascularization (CNV). (**D**) The corresponding OCT B-Scan (scan direction marked by *red arrow* in (**C**)) shows cystoid retinal edema and subretinal tissue (presumably corresponding to subretinal hemorrhage visible on color photos). The RAP lesion itself was not captured by the OCT B-scan.

0.59 mm^3). All 23 eyes showed subretinal tissue on OCT (100%, mean volume 0.37 ± 0.41 mm^3) with 16 cases additionally demonstrating PEDs on OCT as well as occult components on FA (70%, mean volume 0.32 ± 0.36 mm^3). In seven cases (33%), no PED was present on OCT; however, LLUS could be detected on FA in four of those seven cases (57%), indicating occult CNV without RPE elevation.

Occult with no classic CNV (Fig. 3**)** revealed retinal thickening in 21 of 24 cases (88%, mean retinal volume 7.62 ± 0.72 mm^3) and cystoid spaces in 14 cases (58%). Subretinal fluid accumulation was present in 19 eyes (79%, mean volume 0.24 ± 0.5 mm^3). In all cases, PEDs were seen on OCT (100%, mean volume 0.86 ± 0.73 mm^3). Subretinal tissue was additionally present on OCT in seven eyes (29%, mean volume 0.07 ± 0.14 mm^3). In three of those seven eyes, thick subretinal hemorrhage was seen on color photographs. In four eyes, no obvious correlation for the subretinal tissue seen on OCT could be identified on FA or color photographs, despite blocked fluorescence, possibly indicating pigment or other material.

CNV lesions with RAP (Fig. 4**)** showed significant retinal thickening with retinal cystoid spaces in all eight cases (100%, mean retinal volume 8.54 ± 1.76 mm^3). Subretinal fluid was present in four eyes (50%, mean volume 0.42 ± 0.69 mm^3), subretinal tissue in seven eyes (88%, mean volume 0.11 ± 0.1 mm^3) and PEDs in seven eyes (88%, mean volume 0.59 ± 0.62 mm^3).

Area measurements of the total CNV lesion size on fluorescein angiography did not reveal statistically significant differences between lesion type groups (mean area, 3.68 ± 2.69 MPS disc areas for predominantly classic CNV; 3.58 ± 3.01 MPS disc areas for minimally classic CNV; 4.22 ± 2.49 MPS disc areas for occult without classic CNV; and 2.96 ± 2.14 MPS disc areas for CNV with RAP lesions; Figs. 5, 6 and Tables 2, 3).[2]

On OCT, predominantly and minimally classic CNV lesions showed a statistically significant greater volume of subretinal tissue than did occult CNV membranes ($P < 0.001$). Occult with no classic CNV lesions showed a statistically greater PED volume than minimally or predominantly classic cases ($P < 0.001$). Subretinal fluid was most frequently present in predominantly classic CNV; however, there was no statistically significant difference in the volume of subretinal fluid between the different angiographic lesion subtypes. No difference was found between groups regarding total retinal volume and volume of the IHC. However, when comparing the group of occult with no classic CNV cases with eyes containing some

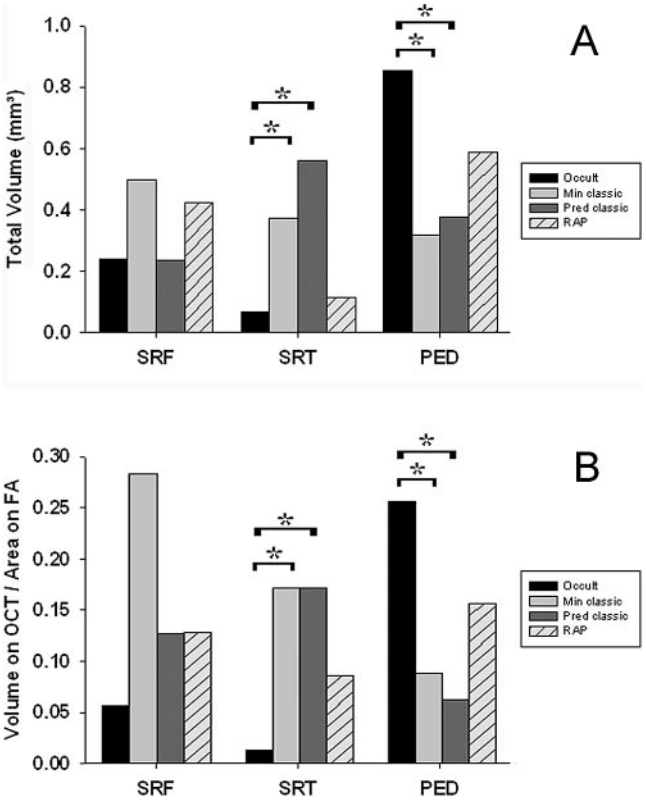

FIGURE 5. Comparison between angiographic lesion subtypes regarding the total volume of the different spaces visible on OCT images. Eyes with classic CNV components showed the largest volume of subretinal tissue, and eyes with occult with no classic CNV showed the largest volumes of PEDs. *Significant difference between groups ($P < 0.001$). (**A**) Total volume values of each space used for analysis. (**B**) Total volume of each space divided by area of the total CNV lesion (volume/area ratio) used for analysis. PED, pigment epithelial detachment; SRF, subretinal fluid; SRT, subretinal tissue.

classic CNV (predominantly and minimally classic cases grouped together), occult with no classic CNV lesions were found to have a significantly lower retinal volume.

DISCUSSION

AMD is a multifactorial disease that presents with a variety of different phenotypes.[1,2,3,15] CNV in neovascular AMD has been classified into classic and occult components based on angiographic characteristics.[2] Classic CNV is believed to correspond histologically to type 2 CNV, which is located in the subretinal space,[6,7] and therefore appears early and sharply demarcated on FA.[2] Leakage of classic CNV progresses throughout the angiogram, as leaking fluid can easily accumulate in the subretinal space (a potential space in the eye) or diffuse through the retinal layers. Occult CNV is believed to correspond histologically to type 1 CNV, which is located in the sub-RPE space.[6,7] The fibrovascular tissue may create disturbances in the overlying RPE, causing occult CNV to often appear as areas of stippled hyperfluorescence on FA.[2] If the outer retinal barrier is disrupted by the disease process, leakage from type 1 CNV may pass through the RPE layer and spread into the subretinal space and/or neurosensory retina. On FA, CNV lesions are classified as predominantly classic CNV, minimally classic CNV, and occult with no classic CNV, based on the proportions of the lesion components classic and occult CNV, thick hemorrhage, blocked fluorescence, and serous PED.[2]

Angiography and OCT represent complementary imaging modalities, both of which display different information. FA reveals information about the integrity of the inner and outer retinal barrier and the presence of pathologic vessels. OCT visualizes the arrangement and reflectivity of retinal and subretinal layers as well as the axial distribution of pathologic fluid or tissue within the retina, the subretinal or sub-RPE space. Interpretation of both imaging modalities together allows for a more precise understanding of disease. For example, a CNV lesion is defined as minimally classic CNV according to the TAP criteria,[2] if classic CNV is visible on FA but other lesion components occupy more than 50% of the total lesion size. Those other lesion components include not only occult CNV, but also blocked fluorescence, thick hemorrhage or serous PED, because these features could obscure the boundaries of CNV. In these cases, OCT could be helpful in confirming or refuting the presence of additional "hidden" CNV, such as the presence of an underlying fibrovascular PED (Fig. 2).

On the other hand, FA may be helpful in the interpretation of subretinal tissue on OCT, as subretinal hyperreflective material on OCT does not necessarily correspond to type 2 CNV, but may be attributed to blood, lipid, fibrin, or pigment, which may appear as blocked fluorescence on FA. As it may not be possible to distinguish CNV from other lesion components of similar reflectivity based on OCT characteristics alone, one OCT grading convention in this study was to assign the generic label "subretinal tissue" to all hyperreflective material identified in the subretinal space. Thus, "subretinal tissue volume" in this study is not equivalent to "type 2 CNV volume."

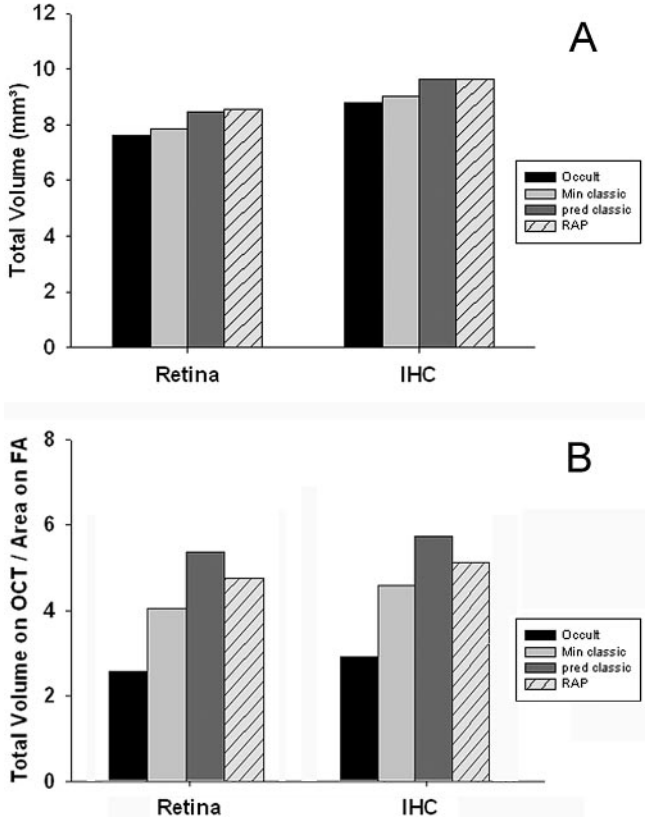

FIGURE 6. Comparison between angiographic lesion subtypes regarding the total volume of the different spaces visible on OCT images. There was no statistically significant difference between groups in the total volume of the retina or the inner retinal height from the choroid (IHC). (**A**) Total volume of each space used for analysis. (**B**) Total volume of each space divided by area of the total CNV lesion (volume/area ratio) used for analysis.

TABLE 3. Volume Ratios of Various Spaces on OCT B-Scans

OCT Parameter	Occult with No Classic (n = 24)	Minimally Classic (n = 23)	Predominantly Classic (n = 11)	RAP Stage III (n = 8)
Retina				
Mean ± SD	2.58 ± 1.92	4.04 ± 3.56	5.37 ± 6.85	4.74 ± 3.46
(min-max)	0.78–9.75	0.72–14.91	1.10–24.53	1.50–10.69
Subretinal fluid				
Mean ± SD	0.06 ± 0.09	0.28 ± 0.39	0.13 ± 0.16	0.13 ± 0.19
(min-max)	0.00–0.30	0.00–1.25	0.00–0.57	0.00–0.48
Subretinal tissue				
Mean ± SD	0.01 ± 0.03	0.17 ± 0.19	0.17 ± 0.10	0.09 ± 0.10
(min-max)	0.00–0.15	0.00–0.79	0.03–0.31	0.00–0.27
PED				
Mean ± SD	0.26 ± 0.25	0.09 ± 0.11	0.06 ± 0.13	0.16 ± 0.13
(min-max)	0.00–0.91	0.00–0.43	0.00–0.44	0.00–0.39
Inner retinal height from choroid				
Mean ± SD	2.90 ± 2.08	4.58 ± 3.93	5.73 ± 7.02	5.12 ± 3.48
(min-max)	0.93–10.56	0.89–16.54	1.44–25.37	2.00–11.04

Volume ratios are the cubic millimeters of each space on OCT/MPS DA of the total CNV lesion on FA.

This study was designed to analyze and compare quantitatively the appearance of various angiographic subtypes of active CNV lesions on OCT. Consistent with our hypothesis, eyes with classic CNV components demonstrated the highest percentage and greatest volume of subretinal tissue on OCT images, whereas eyes with occult with no classic CNV showed the highest percentage and greatest volume of PEDs. This is in accordance with qualitative observations in previously published reports.[9–12] To the authors knowledge, however, this is the first report providing quantitative measurements for comparison of various spaces on OCT other than the neurosensory retina. Interestingly, the mean PED volume in eyes with occult with no classic CNV was higher than in eyes with minimally classic and predominantly classic CNV, although in our series, 20 of 23 eyes with minimally classic CNV and 3 of 11 eyes with predominantly classic CNV appeared to have occult components visible on angiography. One possible explanation for this finding is that occult with no classic CNV lesions (with sub-RPE disease alone) were more likely to grow in the sub-RPE space for an extended period before manifesting with symptoms or other signs, such as a breakthrough of exudation into the subretinal space, prompting diagnosis and treatment.

Intra- and subretinal fluid accumulation have been observed in eyes with angiographically active CNV lesions and have been assumed to be signs of activity.[16–18] Therefore, some studies proposed OCT guided retreatment criteria for neovascular AMD based on retinal volume and presence of subretinal fluid.[17,18] Indeed, in our study, most eyes demonstrated retinal cystoid spaces and/or subretinal fluid accumulation. Four eyes, however, presented with leakage on FA but without subretinal fluid or cystoid spaces on OCT; a finding also described by Eter and Spaide.[19] Three of those four eyes where classified as occult with no classic CNV and one as minimally classic CNV. It seems possible that leakage on FA may not be visible as intra- or subretinal fluid on OCT, if the fluid is pumped out by the RPE just as quickly as it leaks, or if a healthy outer retinal barrier prevents leakage from type 1 CNV from diffusing through the RPE layer. However, since time domain (StratusOCT) imaging captures only a small area of the retina, it is also possible that subretinal fluid or cystoid spaces were in fact present, but not captured by one of the six OCT B-scans. Vice versa, intra- and subretinal fluid accumulation on OCT often correlates with leakage or pooling on FA, but such leakage may not be clearly apparent on the commonly used angiographic time frames (up to 10 minutes), if the source of leakage is very small and leakage is slow. Retinal degeneration in old or chronic CNV lesions may also be associated with loss of neuronal retinal tissue and formation of cystoid spaces without the presence of leakage from active CNV on FA.

In our study, eyes with predominantly classic CNV showed the highest percentage of subretinal fluid. Eyes with occult with no classic CNV demonstrated the lowest percentage of cystoid edema and the smallest volumes of retina and subretinal fluid compared with the other groups. However, there was no significant difference between groups regarding the volume of retina and subretinal fluid. This is in accordance with findings from Hughes et al.,[12] who did not observe a difference in retinal edema and cystoid spaces between eyes with classic and occult CNV. It seems likely that classic CNV may cause retinal or subretinal fluid accumulation, whereas the outer retinal barrier may prevent leakage from occult CNV from passing through the RPE layer in some cases. Occult CNV may eventually induce a breakdown of the outer retinal barrier. RAP lesions in contrast are very likely to show cystoid edema, as leakage from the pathologic vessels (presumed to be intraretinal) can easily diffuse within the retina. In our study, eyes with RAP demonstrated the highest percentage of cystoid edema.

Limitations of this study include the relatively small sample, and the interpolation of data from six radial line StratusOCT B-scans to generate volume data. In addition, in eyes with poor fixation, the six scans will likely not be centered in one point, causing additional errors in volume calculation. The new Fourier domain OCT (FDOCT) devices could address some of these concerns. The high scanning speeds achievable with FDOCT devices confer greater resistance to fixation errors and permit a higher sampling density of the scanned region, requiring less interpolation between sampled locations. Unfortunately, automated segmentation algorithms in FDOCT devices have yet to be validated for complex diseases such as neovascular AMD, and grading every B-scan in a dense FDOCT volume acquisition for a large number of patients is not feasible. Manual correction of a more limited set of scans appears to be a reasonable compromise until the segmentation software associated this new technology matures.

In conclusion, quantitative analysis of OCT images allows for a more precise analysis of anatomic differences between various angiographic subtypes of CNV lesions in neovascular AMD. Quantitative analysis of changes in retinal volume, subretinal fluid, subretinal tissue or PED volumes over time in clinical trials may improve our understanding about differences between classic CNV, occult CNV and RAP in the natural course of the disease or in response to treatment. These findings may also facilitate the development of a new classification

system for CNV lesions which incorporates both angiographic and OCT morphologic characteristics for more precise characterization of lesion subtypes in neovascular AMD.

References

1. Bressler NM, Bressler SB, Congdon NG, et al. Age-Related Eye Disease Study Research Group. Potential public health impact of Age-Related Eye Disease Study results: AREDS report no. 11. *Arch Ophthalmol*. 2003;121:1621–1624.
2. Barbazetto I, Burdan A, Bressler NM, et al. Treatment of Age-Related Macular Degeneration with Photodynamic Therapy Study Group; Verteporfin in Photodynamic Therapy Study Group. Photodynamic therapy of subfoveal choroidal neovascularization with verteporfin: fluorescein angiographic guidelines for evaluation and treatment—TAP and VIP Report No. 2. *Arch Ophthalmol*. 2003; 121:1253–1268.
3. Kuhn D, Meunier I, Soubrane G, et al. Imaging of chorioretinal anastomoses in vascularized retinal pigment epithelium detachments. *Arch Ophthalmol*. 1995;11:1392–89-5208.
4. Brown DM, Kaiser PK, Michels M, et al.; ANCHOR Study Group. Ranibizumab versus verteporfin for neovascular age-related macular degeneration. *N Engl J Med*. 2006;355:1432–1444.
5. Rosenfeld PJ, Brown DM, Heier JS, et al. MARINA Study Group. Ranibizumab for neovascular age-related macular degeneration. *N Engl J Med*. 2006;355:1419–1431.
6. Submacular Surgery Trials Research Group. Comparison of 2D reconstructions of surgically excised subfoveal choroidal neovascularization with fluorescein angiographic features: SST report No. 15. *Ophthalmology.* 2006;113:279.e1–279.e5.
7. Grossniklaus HE, Wilson DJ, Bressler SB, et al. Clinicopathologic studies of eyes that were obtained postmortem from four patients who were enrolled in the submacular surgery trials: SST Report No. 16. *Am J Ophthalmol*. 2006;141:93–104.
8. Fukuchi T, Takahashi K, Uyama M, Matsumura M. Comparative study of experimental choroidal neovascularization by optical coherence tomography and histopathology. *Jpn J Ophthalmol*. 2001; 45:252–258.
9. Sandhu SS, Talks SJ. Correlation of optical coherence tomography, with or without additional colour fundus photography, with stereo fundus fluorescein angiography in diagnosing choroidal neovascular membranes. *Br J Ophthalmol*. 2005;89:967–970.
10. Sato T, Iida T, Hagimura N, Kishi S. Correlation of optical coherence tomography with angiography in retinal pigment epithelial detachment associated with age-related macular degeneration. *Retina*. 2004;24:910–914.
11. Coscas F, Coscas G, Souied E, Tick S, Soubrane G. Optical coherence tomography identification of occult choroidal neovascularization in age-related macular degeneration. *Am J Ophthalmol*. 2007;144:592–599.
12. Hughes EH, Khan J, Patel N, Kashani S, Chong NV. In vivo demonstration of the anatomic differences between classic and occult choroidal neovascularization using optical coherence tomography. *Am J Ophthalmol*. 2005;139:344–346.
13. Sadda SR, Joeres S, Wu Z, Romano P, Collins AT, Walsh AC. Error correction and quantitative sub-analysis of optical coherence tomography data using computer-assisted grading. *Invest Ophthalmol Vis Sci*. 2007;48:839–848.
14. Joeres S, Tsong JW, Updike PG, et al. Reproducibility of quantitative optical coherence tomography sub-analysis in neovascular age-related macular degeneration. *Invest Ophthalmol Vis Sci*. 2007;48:4300–4307.
15. Grossniklaus HE, Green WR. Choroidal neovascularization. *Am J Ophthalmol*. 2004;137:496–503.
16. Kaiser PK, Blodi BA, Shapiro H, Acharya NR. MARINA Study Group. Angiographic and optical coherence tomographic results of the MARINA study of ranibizumab in neovascular age-related macular degeneration. *Ophthalmology.* 2007;114:1868–1875.
17. Fung AE, Lalwani GA, Rosenfeld PJ, et al. An optical coherence tomography-guided, variable dosing regimen with intravitreal ranibizumab (Lucentis) for neovascular age-related macular degeneration. *Am J Ophthalmol*. 2007;143:566–583.
18. van Velthoven ME, de Smet MD, Schlingemann RO, Magnani M, Verbraak FD. Added value of OCT in evaluating the presence of leakage in patients with age-related macular degeneration treated with PDT. *Graefes Arch Clin Exp Ophthalmol*. 2006;244:1119–1123.
19. Eter N, Spaide RF. Comparison of fluorescein angiography and optical coherence tomography for patients with choroidal neovascularization after photodynamic therapy. *Retina*. 2005;25:691–696.